Proceedings of the International Conference on Industrial Engineering and Operations Management

Publisher: IEOM Society International, USA DOI: 10.46254/AP07.20260420
Published: March 25, 2026

Artificial Intelligence-based Prediction of Electrode Life for Resistance Spot Welding Process

Amritesh Kumar, Pranav Jori, Vipin Kumar Mishra and Swarup Bag
Department of Mechanical Engineering
Indian Institute of Technology Guwahati
Guwahati 781039, Assam, India
swarupbag@iitg.ac.in

Brajesh Asati, Nikhil Shajan and Kanwer Singh Arora
Materials Welding & Joining Research Group
Tata Steel Limited, Jamshedpur 831007, India

Abstract

It is almost impossible to develop a wear-free electrode where the practical approach is followed to enhance the electrode life by modulating the process conditions for proper electrode material with geometric design of tip. The degradation of electrode for coated steel mainly occurs due to alloying of pure copper electrode that localize the heat generation randomly and impact on the nugget formation. Hence machine learning (ML) models are developed using cluster-based and feature-based algorithm to outperform the life of three different types of electrodes. Twelve independent features are considered and out of which the nugget diameter is the most sensitive feature on the electrode life. It means the evolution and formation of nugget at optimum weld lobe (range of current and electrode force) decides the number of welds the electrode can perform successfully since the electrode surface condition, specifically for coated steel, is having a direct impact on weld nugget formation. The present analysis shows that almost all ML algorithms performs well for choosing the best feature that impact on resistance spot welding of GA coated high strength bake hardened steel of 0.65 mm thickness.

Keywords
Electrode life, resistance spot welding, Random forest, Artificial neural network, dynamic contact resistance.

1. Introduction
The fundamental understanding of electrode use relies on two aspects: one is the electrode material and design, and other is the efficient process condition. The choice of electrode material is well established and there is not much scope to improve it (Tamizi et al., 2017). The signature parameter is the dynamic contact resistance measurement over weld time It is equally important to look into how the contact resistance between electrode and work piece can be reduced (Wei and Wu, 2012). The secondary aspect of the electrode is the material property, mainly the thermal diffusivity and electrical resistivity. The cooling efficiency depends on the cooling medium, inlet temperature of the cooling medium and the nature of the flow (i.e. degree of turbulence). Moreover, the surface condition changes with repeated use of the electrode (Gedeon and Eagar, 1986). Hence the electrode surface condition with the number of welds is the most important parameter that directly impact on the life of the electrode or optimal utilization of the electrode.

In principle, the degradation of electrode for primary coated steel mainly occurs due to alloying between the sheet coating and the electrode. It is obvious that alloying of pure copper deteriorates the thermal conductivity (or thermal diffusivity) and enhance the electrical resistivity. In contrast, the mechanical properties are improved with alloying of pure copper (Tumuluru, 2007). Investigation by Zou et al. (2005) shows a multi-layer composite coating onto the copper electrode top surface (5 – 10 μm) slightly increases the resistance (7.6%) of the weld system. Chang et al. (2007) shows the electrode pitting morphologies for ring type and hole-type electrodes on RSW of aluminium alloy 5182. When using ring-pitting electrode, the contact radius at faying surface is increased while the current distribution is not affected notably, and the nugget diameter is increased. Zhao et al. (2016) used a disposable flexible strip at the electrode/sheet interfaces (say, 0.12 mm thick Cu55Ni45 alloy strip) for resistance welding of 0.4 mm thick galvanized SAE1004 steel. This method improved the heat generation, lowered the temperature developed at the electrode-sheet interface, and significantly decreases electrode wear. The higher force with shorter weld time has the least contamination on the electrode surface (2016). The roughness of the electrode face is critical to obtain a firm contact with low electric resistance (low heat generation at the EL/WP interface) and extended the electrode life (Zhang et al., 2016). Zhang et al. (2008) characterized the RSW of 0.8 mm thickness galvanization DP600 steel. The wear rate (high deformation) were higher at the earlier stage.

Investigation on the diffusion of coating and alloy layer thickness on electrode surface in both static and dynamic conditions is also a measure to understand the life expectancy of the electrode material. The setting of optimum welding parameters (current, weld time, electrode-holding time) under continuous or pulse current to ensure minimum weld nugget size at minimum weld current ((Feujofack Kemda et al., 2022, Chen et al., 2019)

There are several ways to apply online monitoring system tracking to the dynamic contact resistance for a better representation of electrode-substrate interaction (Butsykin et al., 2023). The use of electrode signals mainly the displacement of electrodes over repetitive use of spot welding is useful to predict the electrode life (Panza et al., 2022)

There are several ML and deep learning algorithms used in the analysis of resistance spot welding process (Panza et al., 2022, Dai et al., 2022, Pham et al., 2022). With the analysis of the influencing factors on the life of electrode, total 11 parameters are identified that actually impact on the electrode life. The spot-welding experiments are conducted on GA coated high strength bake hardened steel of 0.65 mm thickness with reference to these influencing parameters. The experimental data are evaluated in a gap of 100 spots. A proper data structure is formed with reference to different ML algorithms where the output is the number of welds. Both ANN and RF algorithms are considered after several trials that comply with the present data structure. The correlation of the type of electrodes (mainly different in geometric shape) with the number of welds is also established using both RF and ANN model. The performance of both the algorithms are also analysed and further tested on the unknown data. The comparison of the predicted value with the experimental one indicates the reliability of the present model.

2. Materials and methods

Bake hardening steel BH340 of thickness 0.65 mm was used in this study. The sheets are galvannealed with a coating weight of 45 gsm on each side to improve scratch resistance, spot weldability and formability. The chemical composition of the material is determined using optical emission spectroscopy and is presented in Table 1.

Table 1. Chemical composition (wt.%) of as received sheet.

Steel	C	Mn	S	P	Si	Al	B	MO	Ni	Nb	Ti	Fe
BH340 (0.65 mm)	0.0018	0.469	0.008	0.048	0.004	0.048	0.0001	0.029	0.01	0.005	0.001	Bal.

2.1 Resistance spot welding experiments

RSW experiments were performed to generate weld data using a 150-kVA pedestal medium frequency direct current machine with dome-shaped electrode geometry having a tip diameter of 6 mm and truncated cone electrode having a tip diameter of 6 mm. Electrode force, weld time, and hold time are considered as 2.94 kN, 240 ms and 80 ms, respectively. A weldability lobe is developed satisfying the minimum nugget diameter criteria (= $4\sqrt{t}$ where t is thickness in mm). The welding schedules are designed for double pulse welding by varying the weld current, the number of pulses and a time lapse between two cycles. For pre-pulse welding, at first, squeeze time is given for 400 ms, after that, the pre-pulse current of 80% of main current is applied for 30 ms. while main pulse is applied for 240 ms. The size of the electrodes and the force are kept constant for welding schedules. The temperature of water flow through electrode was at 25˚C and its flow rate was 4 L/min for cooling the electrodes (Böhne et al., 2020, Ashiri et al., 2018).

In electrode life test electrode made of copper–chromium–zirconium alloy with flat dome shape, ring dome and truncated cone electrode were used. Electrode life was evaluated using AWS D8.9 standard(American Welding Society, 2012).

In the electrode life test, welds are applied at current just below the I_{max} value and the weld diameters of the last 7 spot welds are measured for every 100 spot welds for truncated cone, ring dome and flat dome shape electrode. Measurement of the weld diameter continues until the number of spots reaches 1100, and the test is terminated when the weld diameter reaches the minimum weld diameter value (= $4\sqrt{t}$ where t is thickness in mm). Carbon imprints were taken for both lower and upper electrodes and combination of both. **Table 2** depicts the parameters used for electrode life test**.**

Table 2. Weld parameter used for electrode life testing

Electrode	**Pre-Pulse**				**Main Pulse**	
	Weld current (kA)	Weld Time (ms)	Electrode force (kN)	Cooling Time (ms)	Weld current (kA)	Weld Time (ms)
Flat dome	6.8	30	2.94	35	8.5	240
Truncated dome	7.2	30	2.94	35	9	240
Ring dome	7.2	30	3.94	35	9	240

2.2 Prediction model

An experimental dataset from resistance spot welding (RSW) operations was mainly used for prediction of two key performance indicators i.e. nugget diameter and electrode life (represented as the number of welds). The input features included pre-pulse welding current, main welding current, weld time, mean DCR along with derived MDCR parameters. To ensure the integrity and reliability of the dataset, preliminary data preprocessing was conducted. The Pearson correlation matrix was employed to evaluate the degree of linear association among the features and to remove highly correlated variables, thereby minimizing redundancy in model training. To capture hidden patterns and group similar welding conditions, K-means clustering was applied to the pre-processed data. The optimal number of clusters (K) was determined through an iterative evaluation of the silhouette coefficient. An artificial intelligence (AI)-based framework, referred to as the Cluster-Integrated Regression Model (CIRM), was developed to predict both electrode life and nugget diameter. The CIRM approach combines the advantages of clustering with supervised regression learning to achieve robust prediction accuracy across varying weld conditions. Figure 1 depicts the overall utilization of the algorithms.

Model training and testing were carried out using a 5-fold cross-validation strategy to ensure generalizability and minimize overfitting. Several regression algorithms and ensemble methods were evaluated and benchmarked using standard performance metrics, including the coefficient of determination (R^2), root mean square error (RMSE), and mean absolute error (MAE), The trained models were validated against unseen experimental data to assess their predictive capability. A linear fit analysis was performed to evaluate the consistency of the cluster-based predictions, confirming the model's stability and reliability under varying process conditions. To enhance the interpretability of the predictive framework, feature importance and sensitivity analyses were conducted. A Pareto analysis identified the dominant input parameters influencing electrode life and nugget formation. Further insights were obtained using the shapely Additive explanations (SHAP) method, which quantified the contribution of each input variable to the model's output predictions.

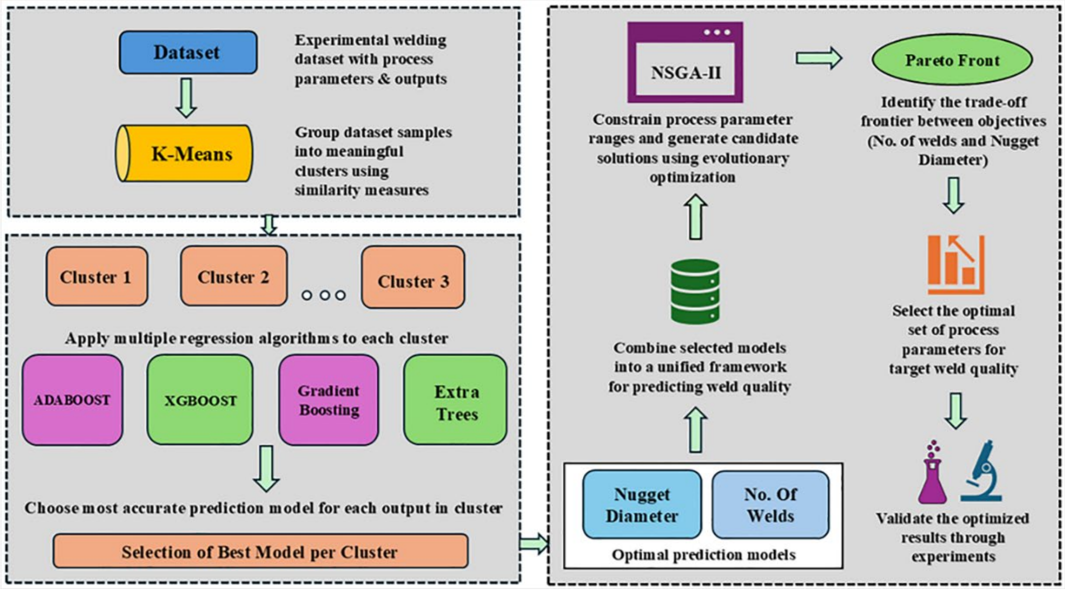

Figure 1. Schematic illustration of the sequential steps involved in predicting the nugget diameter and number of welds.

3 Results and discussions

Figure 2 illustrates the Pearson correlation matrix, emphasizing the key relationships between current, resistance, timing, and geometric parameters, offering a visual validation of the numerical correlations mentioned. The correlation map reveals a tightly coupled electrical subsystem and clear geometric–electrical trade-offs. The two current channels are essentially the same control knob: pre-pulse current and main weld current are almost perfectly correlated ($r \approx 1.00$), and both scales almost identically with heat input ($r \approx 0.95$), confirming that energy delivery is governed primarily by current magnitude. Within the pulse-1 electrical metrics, form a strongly coherent triad, indicating that higher instantaneous resistance coincides with larger resistance peaks and higher average dynamic contact resistance consistent with localized heating and constriction effects.

In contrast, electrode geometry exhibits pronounced inverse relations with resistance features. Similarly, the fixed electrode diameter shows strong negative correlations with pulse-1. Mechanistically, larger contact areas reduce constriction resistance, suppressing peak and mean DCR values. Finally, Mean DCR (pulse-2) is negatively related to both current channels, suggesting that increasing current and thus heat input can reduce measured dynamic resistance through softening and improved contact, even as pulse-1 peak metrics rise. This reveals the competing roles of geometry (contact area) and current (heating intensity). Overall, these numerical correlations indicate strong multicollinearity among currents, heat input, and resistance features, especially within and across pulses, while electrode diameters act as stabilizing, oppositely directed factors.

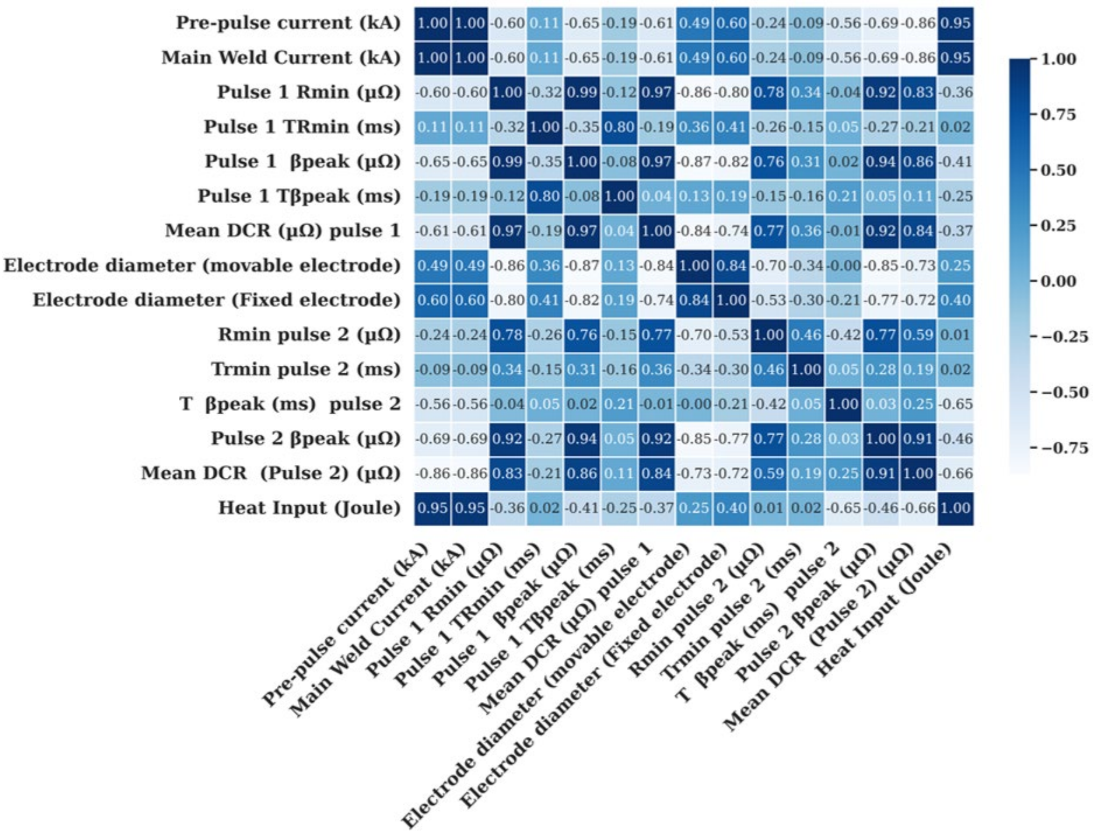

Figure 2. Analysis of the linearity between features using Pearson correlation matrix.

3.1 K-means algorithm results

The K means analysis on the 409 standardized samples yields a clear optimum at three clusters based on the silhouette curve, with scores k = 2 → 0.673, k = 3 → 0.678, k = 4 → 0.545, and k = 5 → 0.563, so k = 3 provides the most compact and well separated partition of the data (Figure 3). Fixing k = 3 and projecting the features confirms this structure in both principal component analysis and t SNE, where the three groups appear as compact islands with clean convex boundaries, indicating that the separation is robust under linear and non-linear embeddings and is not an artifact of a single view.

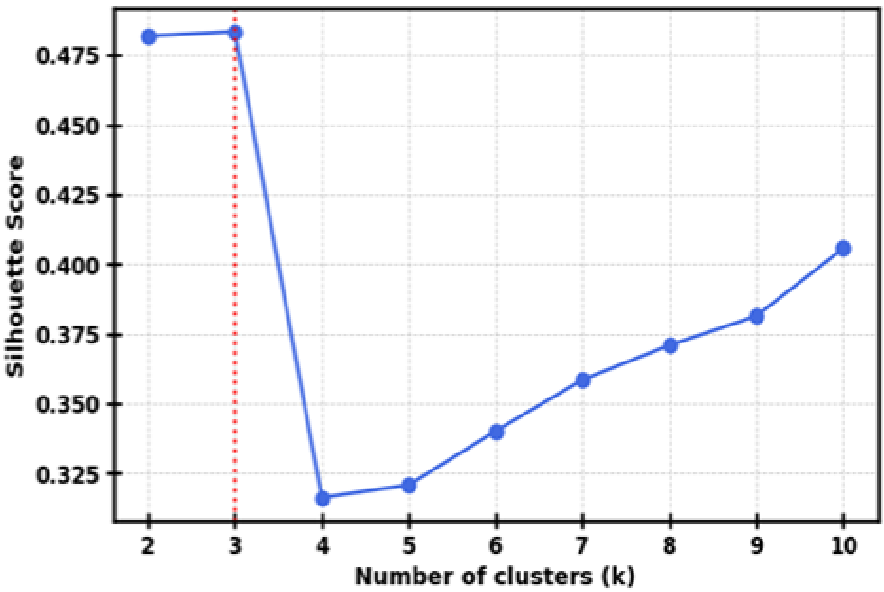

Figure 3. Evaluation of K value using K-means algorithm and obtained results from K-means clustering.

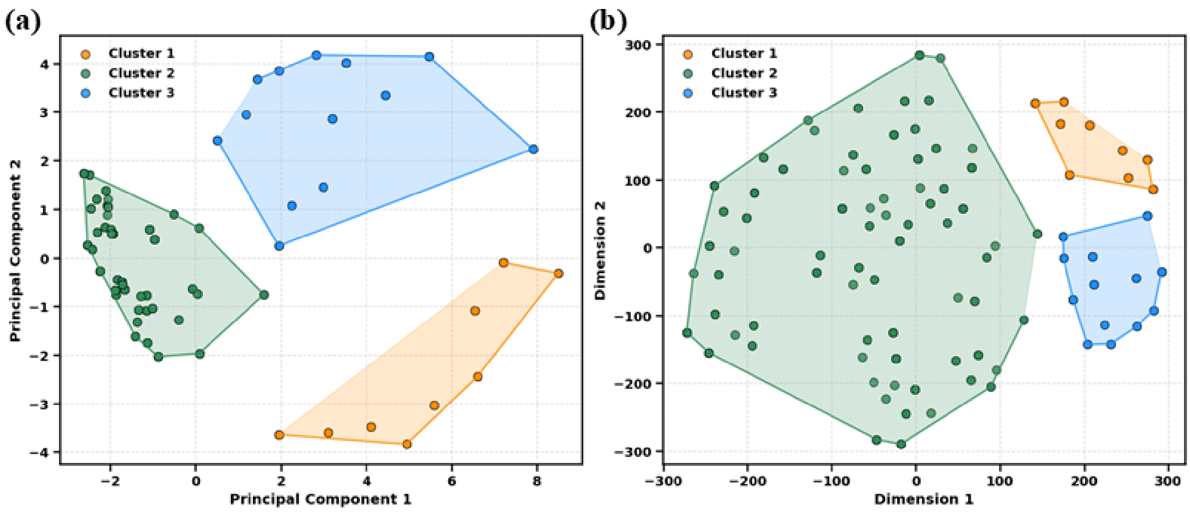

Figure 4. (a) variation of the silhouette coefficient for cluster numbers and (b, c) two-dimensional visualization of the clustering results corresponding to the optimal clusters.

This behavior is clearly visible in Figure 6, where the PCA (**Figure 4a**) illustrates three clusters arranged along understandable variance axes, while the t-SNE projection (**Figure 4b**) emphasizes the maintenance of local–global neighborhoods and distinctly separated cluster boundaries. The agreement between PCA and t-SNE further strengthens the physical separability of the dataset. No of welds and Nugget Dia and training cluster specific models on a four to one split to capture the localized parameter to response relationships more accurately than a single global model.

3.2 Selection of optimal regressor model for clustering

To determine the most suitable and generalizable predictive framework across all identified process clusters, a multi-objective optimization approach was implemented using the NSGA-II algorithm. This strategy was adopted to jointly minimize the root mean square error (RMSE) for both the number of welds and nugget diameter, thereby ensuring that the final model configuration achieved balanced accuracy across the two dependent variables. Figure 5 depicts 5-fold cross-validation fitness for two targets, with the mean shown as a bar and the fold-to-fold spread shown as an error bar. For number of welds, the average fitness is 95%, with an error bar of ±80%. This mean exceeds the target threshold of 90% indicated by the horizontal reference line, suggesting that the model can reach high accuracy on some folds. The very widespread, however, indicates strong instability across splits, consistent with heterogeneous fold composition, sensitivity to influential observations, or cluster imbalance. In practical terms, performance for number of welds is promising on average but not yet reliable without stabilizing the training and evaluation criteria. For nugget diameter, the average fitness is 5% with a narrow error bar of ±2%. This level is far below the 90% threshold and signals that the current representation and modelling choices are not capturing the governing relationships for this response. As one replaces the placeholder values with metrics computed directly from your folds, report both the mean and dispersion with exact numeric as done here, and retain the 90% reference line to make threshold attainment visually explicit.

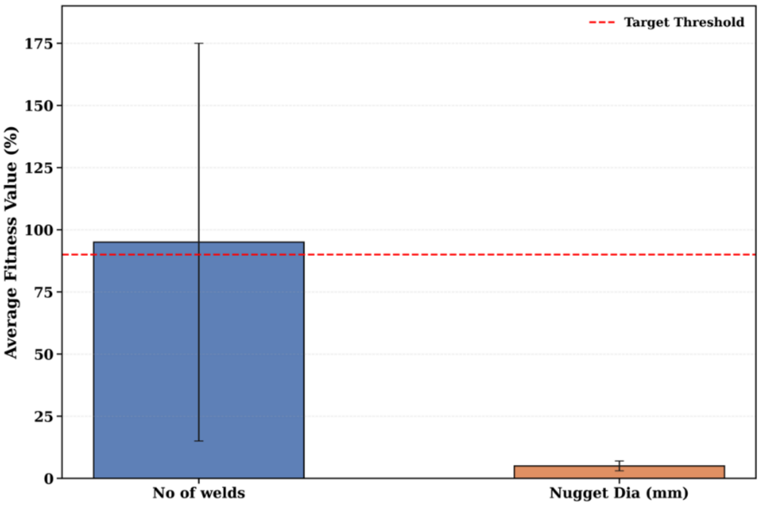

Figure 5. Average fitness values of CIRM for the prediction of electrode characteristics evaluated using 5-fold cross-validation.

Figure 6 compares the coefficient of determination for both responses across the three data regimes defined by clustering and shows that ensemble learners recover most of the explainable variance in weld quality. The near unity values are consistent with a narrow spread of conditions and with features that closely represent the governing physics, for example heat input, resistance minima and peaks, and pulse timing. Cluster 1 provides the most stringent test because it is the largest and most heterogeneous regime. Even here, accuracy remains very high. The slight advantage of XGB for weld count is consistent with gradient boosted trees exploiting residual structure through sequential fitting and shrinkage, which helps capture weak interactions among main current, pulse duration, and dynamic contact resistance. The near parity among the three methods for nugget diameter implies that the chosen descriptors already capture most of the thermal and geometric determinants of nugget growth in this regime.

Cluster 2 shows the only modest reduction in predictive precision for number of welds. This small drop likely reflects higher stochasticity due to process phenomena that are harder to encode, such as transient contact conditions, partial electrode wear, or localized heat distribution effects. As with Cluster 0, these perfect values require verification with stratified cross validation and feature family ablation to rule out target degeneracy. Taken together, the panels show that the cluster informed strategy isolates regimes with consistent physics, allowing ensemble regressors to achieve R^2 between 0.912 and 1.000 for number of welds and up to 1.000 for nugget diameter. Cluster 1 results provide strong evidence of generalization under realistic variability, while the perfect scores for nugget diameter in Clusters 0 and 2 should be validated with repeated, cluster aware cross validation and by auditing features derived from dynamic resistance and pulse timing.

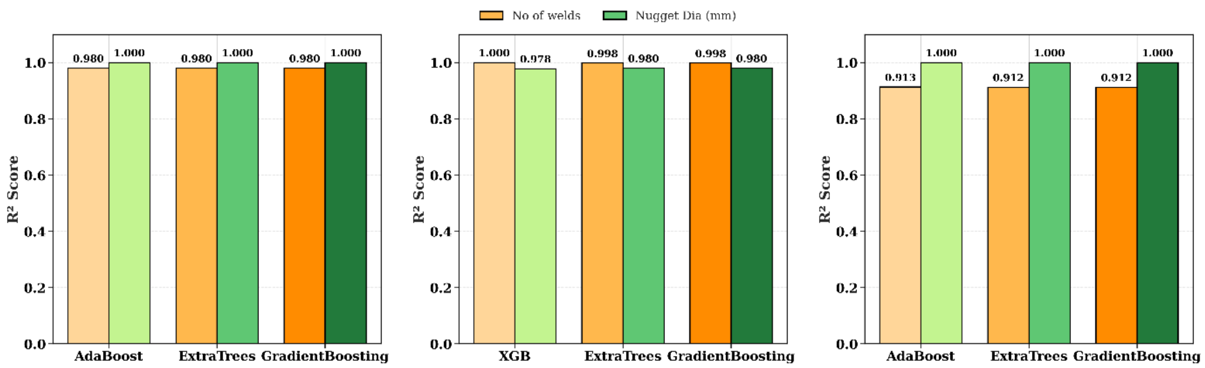

Figure 6. Maximum and minimum values of R^2 for each cluster for the prediction of Number of welds and nugget diameter.

3.3 Influence of K-means on model performance

Figure 7 depicts the cohesive interpretation of the linear-fit "predicted vs actual" curves for number of welds, using your reported statistics. First, the test-set panels show that tree-based ensembles and the CIRM pipeline reproduce weld counts with essentially perfect fidelity. In a linear-fit view, these figures correspond to point clouds that collapse onto the 45° identity line, with fitted regression lines whose slope is effectively 1 and intercept is effectively 0. The vanishing MAE indicates that the absolute prediction error is well below one weld across the entire testing range, which is stronger than typical process control tolerances. Scientifically, such behaviour is consistent with a response that is strongly constrained by the measured inputs. The combination of current levels, pulse timing, dynamic resistance features, and heat input appears sufficient to reconstruct the weld count deterministically once the data are stratified. Training-set performance is also extremely strong for the boosted and bagged trees, albeit with slightly larger absolute errors than on the test set. The CIRM curve being the tightest of the three is consistent with its cluster-aware fitting that reduces within-regime heterogeneity before modelling.

The AdaBoost results implies a linear fit that remains close to the identity line but with visibly larger spread than the other ensembles. A training MAE that is two orders of magnitude larger than the test MAE is unlikely if both are computed on the same target scale and with the same preprocessing. In a linear-fit panel, such a number would imply either a handful of extreme outliers far from the identity line or a scaling issue. If the panel shows a few distant points while most lie on the line, a robust metric such as median absolute error and an influence analysis would clarify whether a small number of high-leverage cases dominate the error. Taken together, the linear fits indicate that model bias is essentially zero for XGBoost, ExtraTrees, and CIRM and very small for AdaBoost on the test set. From a process standpoint, this means that the chosen features capture the dominant electro-thermal determinants of weld count. From a modeling standpoint, the cluster-informed strategy used by CIRM removes cross-regime heterogeneity, which explains why its training MAE is the smallest among the three and its test panel is indistinguishable from the identity line.

Figure 8 displays the linear-fit curves that contrast the predicted and actual values for both responses throughout all cluster-based models. The data points in both graphs align nearly exactly with the 45° identity line, showing minimal bias and very slight residual variation. The slope and intercept of the fitted lines are essentially 1 and 0, respectively, verifying that the cluster-specific models accurately reflect the true values with nearly deterministic precision. The very close alignment additionally visually reinforces the elevated R^2 and minimal MAE values documented for these models.

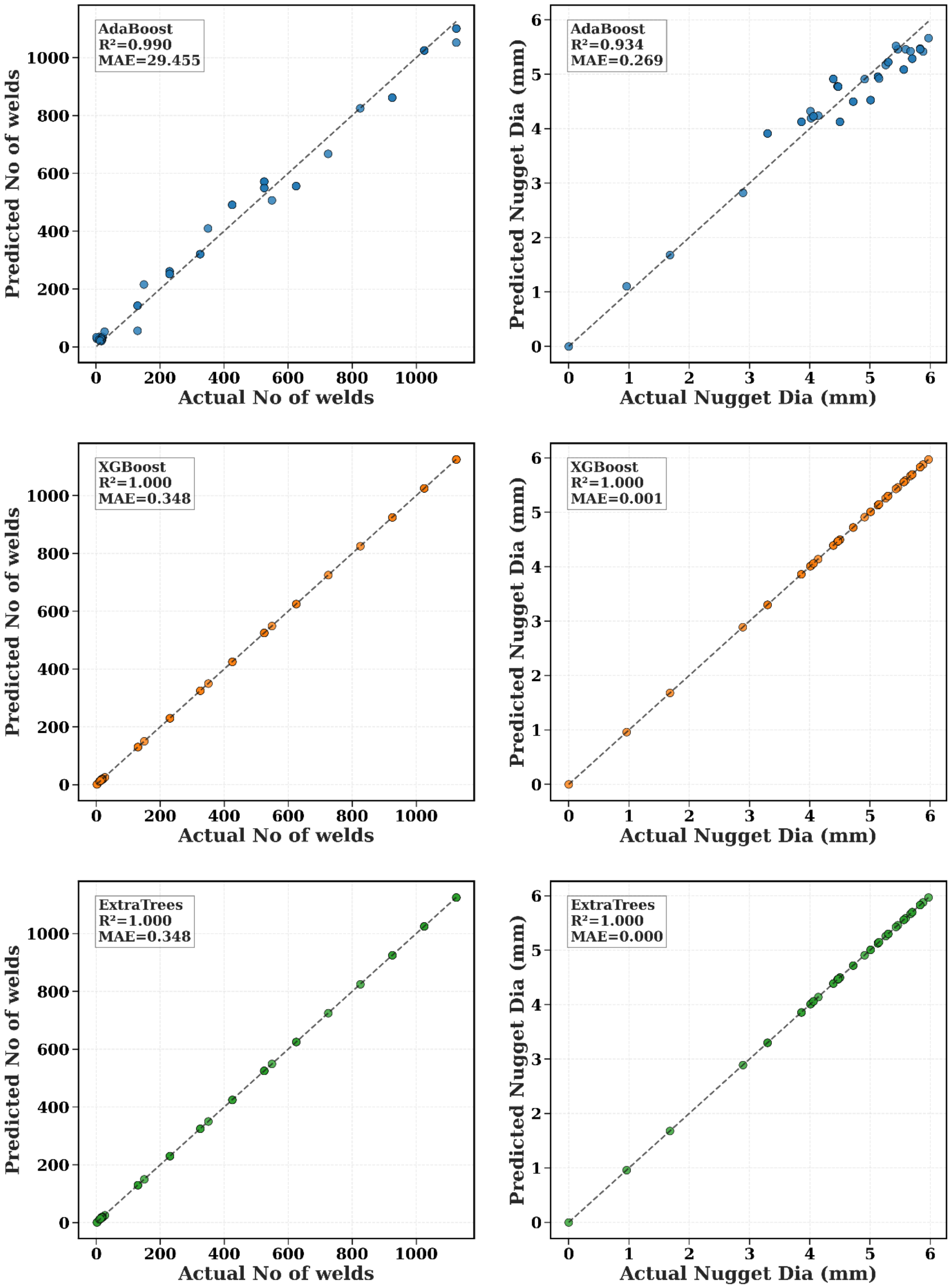

Figure 7. Comparison between predicted and actual no of welds (a, b, c) and predicted nugget diameter (d, e, f).

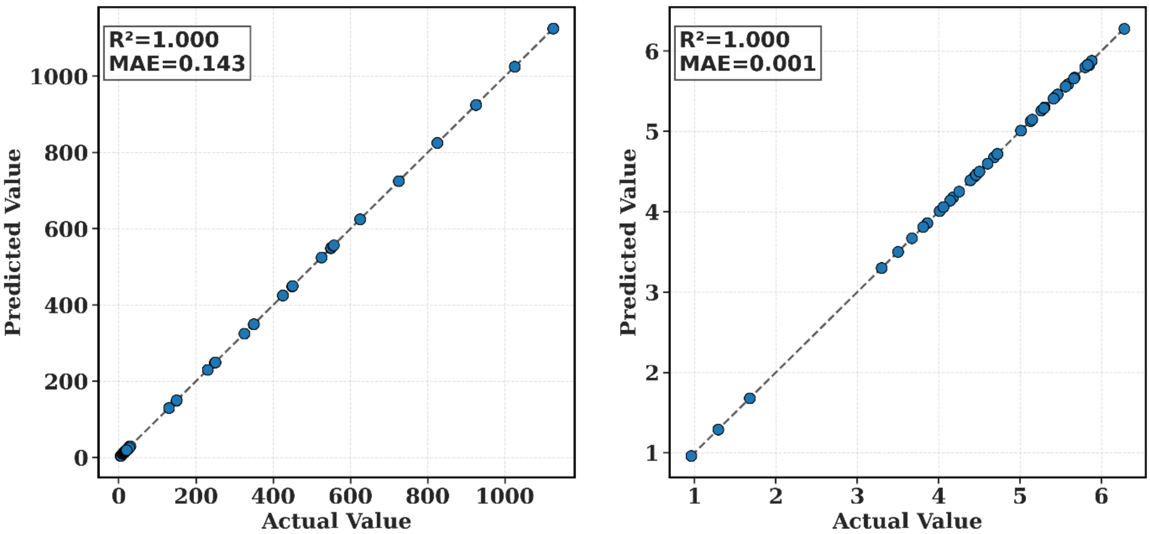

Figure 8. Linear fit curve of cluster algorithms.

3.4 Influence of welding attributes on electrode life

The steadily ascending Pareto front indicates that enhancing both current and heat input at the same time leads to better results in the performance metrics. Regarding the count of welds, the diameter of the fixed-side electrode, Rmin (pulse 2), and β-peak (pulse 2) appear as the most significant influences. The fixed electrode diameter and pulse-2 resistance attributes prevail, where majority of the predictive contribution for nugget diameter comes from the β-peak and electrode diameters. When the electrode diameter grows, a positive impact on the lifespan of the electrode is observed, whereas increased heat input results in decrease of electrode lifespan due to excessive thermal stress.

4. Conclusions

In the current work, the clustering-integrated ensemble learning model (CIELM) is coupled with the non-dominated sorting genetic algorithm II (NSGA-II) to optimize the conflicting objectives of electrode life and weld nugget diameter in resistance spot welding. By leveraging K-Means clustering to partition the high-dimensional parameter space into physically relevant operational regimes, the model achieved unprecedented predictive accuracy. The subsequent NSGA-II optimization successfully generated a comprehensive Pareto front, providing manufacturers with a complete map of non-dominated solutions. The application of clustering proved instrumental in accurately modeling the highly non-linear dynamics associated with electrode wear. By isolating distinct wear regimes, the CIELM bypassed the typical degradation in accuracy experienced by global models. The optimization process yielded a practical set of optimal solutions, demonstrating that the Truncated Cone electrode geometry provides the best balance for maximizing life while maintaining quality. Investigating the applicability of transfer learning techniques would significantly expand the framework's utility. By treating the CIELM weights derived from a specific electrode material (e.g., the current copper alloy data) as initial starting points for modeling a new material, the time and cost required to deploy the model for new RSW applications could be drastically reduced, leveraging the domain knowledge acquired in the current study.

References

American Welding Society, *Test methods for evaluating the resistance spot welding behavior of automotive sheet steel materials*, 2012.

Ashiri, R., Marashi, S.P.H. and Park, Y.D., Weld processing and mechanical responses of 1-GPa TRIP steel resistance spot welds, *Welding Journal*, vol. 97, no. 5, pp. 157S–169S, 2018.

Böhne, C., Meschut, G., Biegler, M. and Rethmeier, M., Avoidance of liquid metal embrittlement during resistance spot welding by heat input dependent hold time adaption, *Science and Technology of Welding and Joining*, pp. 617–624, 2020.

Böhne, C., Meschut, G., Biegler, M., Frei, J. and Rethmeier, M., Prevention of liquid metal embrittlement cracks in resistance spot welds by adaption of electrode geometry, *Science and Technology of Welding and Joining*, vol. 25, no. 4, pp. 303–310, 2020.

Butsykin, S., Gordynets, A., Kiselev, A. et al., Evaluation of the reliability of resistance spot welding control via on-line monitoring of dynamic resistance, *Journal of Intelligent Manufacturing*, vol. 34, pp. 3109–3129, 2023. https://doi.org/10.1007/s10845-022-01987-0

Chang, B.H., Du, D., Chen, Q. and Zhou, Y., Studies on effects of pitting morphology in resistance spot welding of aluminium alloy, *Science and Technology of Welding and Joining*, vol. 12, no. 1, pp. 67–72, 2007. https://doi.org/10.1179/174329306X147526

Chen, F., Wang, Y., Sun, S. et al., Multi-objective optimization of mechanical quality and stability during micro resistance spot welding, *International Journal of Advanced Manufacturing Technology*, vol. 101, pp. 1903–1913, 2019. https://doi.org/10.1007/s00170-018-3055-x

Dai, W., Li, D., Tang, D., Wang, H. and Peng, Y., Deep learning approach for defective spot welds classification using small and class-imbalanced datasets, *Neurocomputing*, vol. 477, pp. 46–60, 2022. https://doi.org/10.1016/j.neucom.2022.01.004

Dai, W., Li, D., Zheng, Y., Wang, D., Tang, D., Wang, H. and Peng, Y., Online quality inspection of resistance spot welding for automotive production lines, *Journal of Manufacturing Systems*, vol. 63, pp. 354–369, 2022. https://doi.org/10.1016/j.jmsy.2022.04.008

Feujofack Kemda, B.V., Barka, N., Jahazi, M. et al., Multi-objective optimization of process parameters in resistance spot welding of A36 mild steel and hot dipped galvanized steel sheets using non-dominated sorting genetic algorithm, *Metals and Materials International*, vol. 28, pp. 487–502, 2022. https://doi.org/10.1007/s12540-021-00986-9

Gedeon, S.A. and Eagar, T.W., Resistance spot welding of galvanized steel: Part II—Mechanisms of spot weld nugget formation, *Metallurgical Transactions B*, vol. 17, no. 4, pp. 887–901, 1986. https://doi.org/10.1007/BF02657152

Panza, L., Maddis, M.D. and Spena, P.R., Use of electrode displacement signals for electrode degradation assessment in resistance spot welding, *Journal of Manufacturing Processes*, vol. 76, pp. 93–105, 2022. https://doi.org/10.1016/j.jmapro.2022.01.060

Pham, V.H., Vo, T.H., Vu, D.D., Choi, J., Park, S., Nguyen, D.T., Lee, B.-I. and Oh, J., Development of scanning acoustic microscopy system for evaluating the resistance spot welding quality, *Research in Nondestructive Evaluation*, vol. 33, no. 3, pp. 123–137, 2022. https://doi.org/10.1080/09349847.2022.2073415

Tamizi, M., Pouranvari, M. and Movahedi, M., Welding metallurgy of martensitic advanced high strength steels during resistance spot welding, *Science and Technology of Welding and Joining*, vol. 22, no. 4, pp. 327–335, 2017. https://doi.org/10.1080/13621718.2016.1240979

Tumuluru, M., The effect of coatings on the resistance spot welding behavior of 780 MPa dual-phase steel, *Welding Journal*, vol. 86, no. 6, pp. 161s–169s, 2007. https://app.aws.org/wj/supplement/WJ_2007_06_s161.pdf

Wei, P.S. and Wu, T.H., Electrical contact resistance effect on resistance spot welding, *International Journal of Heat and Mass Transfer*, vol. 55, no. 11–12, pp. 3316–3324, 2012. https://doi.org/10.1016/j.ijheatmasstransfer.2012.01.040

Yurioka, N., Comparison of preheat predictive methods, 2004.

Zhang, W.J., Cross, I., Feldman, P., Rama, S., Norman, S. and Del Duca, M., Electrode life of aluminium resistance spot welding in automotive applications: a survey, *Science and Technology of Welding and Joining*, vol. 22, no. 1, pp. 22–40, 2016. https://doi.org/10.1080/13621718.2016.1180844

Zhang, X.Q., Chen, G.L. and Zhang, Y.S., Characteristics of electrode wear in resistance spot welding dual-phase steels, *Materials & Design*, vol. 29, pp. 279–283, 2008. https://doi.org/10.1016/j.matdes.2006.10.025

Zhao, Y.Y., Zhang, Y.S., Lai, X.M. and Wang, P.C., Resistance spot welding of ultra-thin automotive steel, *Journal of Manufacturing Science and Engineering*, vol. 135, pp. 021012-1–021012-10, 2013. https://doi.org/10.1115/1.4023367

Zou, J., Zhao, Q. and Chen, Z., Surface modified long-life electrode for resistance spot welding of Zn-coated steel, *Journal of Materials Processing Technology*, vol. 209, pp. 4141–4146, 2009. https://doi.org/10.1016/j.jmatprotec.2008.10.005